Nano Res. 2011, 4(10): 987–995
DOI 10.1007/s12274-011-0155-4
Research Article

ISSN 1998-0124
CN 11-5974/O4

Spatially Resolved Photoelectric Performance of Axial GaAs Nanowire pn-Diodes

Andrey Lysov (✉), Sasa Vinaji, Matthias Offer, Christoph Gutsche, Ingo Regolin, Wolfgang Mertin, Martin Geller, Werner Prost, Gerd Bacher, and Franz-Josef Tegude

Center for Nanointegration Duisburg-Essen, University of Duisburg-Essen, 47048, Duisburg, Germany

Received: 13 April 2011 / Revised: 26 May 2011 / Accepted: 28 May 2011

ABSTRACT

The spatially resolved photoelectric response of a single axial GaAs nanowire pn-diode has been investigated with scanning photocurrent and Kelvin probe force microscopy. Optical generation of carriers at the pn-junction has been shown to dominate the photoresponse. A photocurrent of 88 pA, an open circuit voltage of 0.56 V and a fill factor of 69% were obtained under AM 1.5 G conditions. The photocurrent followed the increasing photoexcitation with 0.24 A/W up to an illumination density of at least 90 W/cm^2, which is important for potential applications in concentrator solar cells.

KEYWORDS

GaAs, nanowire, solar cells, scanning photocurrent microscopy, Kelvin probe force microscopy, electroluminescence

1. Introduction

In recent years, semiconductor nanowires have attracted considerable attention for the fabrication of nanoscale optoelectronic devices. The nanowire approach allows for a combination of highly mismatched Ⅲ–Ⅴ compound semiconductors [1–4] and their co-integration with standard silicon technology [5, 6]. The enhanced light collection efficiency with respect to conventional thin film devices [7, 8] together with the freedom of integrating multiple p–n junctions with optimized spectral response to the solar spectrum [9, 10] makes Ⅲ–Ⅴ nanowires quite attractive for the development of high performance photovoltaic (PV) devices.

The material mostly used for PV nanowire devices is Si [7, 11, 12]. Intensive research efforts over the last few years have led to an open circuit voltage of V_{oc} = 519 mV, a short circuit current density of J_{sc} = 16.8 mA/cm^2, a fill factor of FF = 61% and an efficiency of η = 5.3% being reported for Si core–shell nanowire pn-diode arrays [7]. Tandem homojunction PV devices were demonstrated for axial Si nanowire pin-diodes, in which Si nanowire tunnel diodes were used to connect single p–i–n-junctions in series [12].

In contrast to Si, Ⅲ–Ⅴ compound semiconductors (i) are often direct semiconductors implying significantly enhanced absorption coefficient, (ii) have bandgaps spanning a wide spectral range, and (iii) allow for overcoming the Shockley–Queisser limit by tandem approaches, which facilitates integration of multiple hetero junctions into a single device [13]. In layered thin film devices, however, their flexibility is limited by strain restrictions. This has strongly triggered efforts

Address correspondence to andrey.lysov@uni-due.de

to develop Ⅲ–Ⅴ nanowire PV devices having either axial or radial pn-junctions [9, 10, 14–18].

Planar concentrator multijunction solar cells with efficiencies exceeding values of 30% are often based on GaAs subcells, as GaAs allows for lattice-mismatched growth on Ge [19]. Furthermore, its bandgap (1.42 eV) makes it suitable for the use as middle subcell on which GaInP- or AlGaInP-based top subcells can be grown lattice-matched [19, 20]. Therefore, there is an immense interest in the realization of GaAs based nanowire-PV devices.

Until now, however, only a few successful demonstrations of GaAs-nanowire PV devices have been reported. For this type of nanowire device, efficiencies ranging from 0.83% [18] for coaxial nanowire diode arrays up to 4.5% [17] for a single coaxial nanowire diode have been reported. Axial p–n nanowires, in contrast, allow multijunction devices to be fabricated more easily than core–shell approaches. In addition, they are expected to exhibit lower leakage currents and therefore should possess a superior rectifying behavior compared to radial p–n junction nanowire diodes. However, to date there have been no reports of the photovoltaic performance of axial GaAs nanowire PV devices.

In this work we investigate the photoelectric performance of single axial nanowire pn-diodes using scanning photocurrent and Kelvin probe force microscopy. These techniques enable us to visualize an axial doping modulation, to determine the extension of the depletion region and to localize the position of maximal photoresponse in a single nanowire pn-junction.

2. Experimental

Axial nanowire pn-junctions were synthesized via the Au-nanoparticle catalyzed vapor–liquid–solid (VLS) growth method by use of low pressure metalorganic vapor phase epitaxy (MOVPE) (50 mbar). Axial modulation of the doping was achieved by subsequent switching of doping precursors without any growth interruptions. A mean hole concentration of 2×10^{19} cm^{-3} was realized with zinc for p-doping, while n-doping with a mean electron concentration of 1×10^{18} cm^{-3} was obtained using tin. The carrier concentrations in the nanowires were determined by a mobility vs. carrier concentration model discussed elsewhere [21, 22].

The as-grown pn-junctions were of zinc blende structure with few stacking faults. No structural change was observed along the whole length of the nanowire diodes. Since the axial growth rate was at least 1500 times higher than the radial growth rate, the typical nanowire diodes investigated here were practically non-tapered. More details about the growth and the structural properties of the nanowire pn-junctions can be found in the literature [23].

For the optoelectronic characterization the nanowires were scratched off the substrate, dispersed in isopropyl alcohol and transferred to pre-patterned insulating substrates. Electrical contacts were defined by electron beam lithography and evaporation techniques. Pt/Ti/Pt/Au was used to contact the p-GaAs nanowire area. To achieve ohmic contact behavior, rapid thermal annealing was carried out at 360 ˚C for 30 s. Pd/Ge/Au annealed for 30 s at 280 ˚C was used as an ohmic contact for the n-doped nanowire area. In this work, measurements on two typical nanowire diodes D1 and D2 are presented. Nanowire diodes D1 and D2, respectively had diameters of 200 nm and 100 nm, and nanowire lengths of 16 μm and 12.5 μm between the electrical contacts.

3. Results and discussion

For a first demonstration of the device performance of the axial nanowire pn-diode, the electroluminescence of a forward biased nanowire pn-diode was monitored at 300 K using an optical microscope. A liquid N_2-cooled charge-coupled device (CCD) camera operating in an imaging mode was used as a detector. The setup and a SEM picture of the nanowire diode D1 are shown in Fig. 1(a). Figure 1(b) shows a CCD camera image of the diode biased at 3 V in the forward direction. To highlight the position of the contacted nanowire, the sample was illuminated by scattered light from the side. Bright electroluminescence directly at the pn-junction was observed for the contacted nanowire. The intensity of light emission increased with the applied bias, showing a threshold voltage of 1.4 V (see the video in the Electronic Supplementary Material (ESM)). The light emission lies in the near infrared range of 1.4–1.5 eV

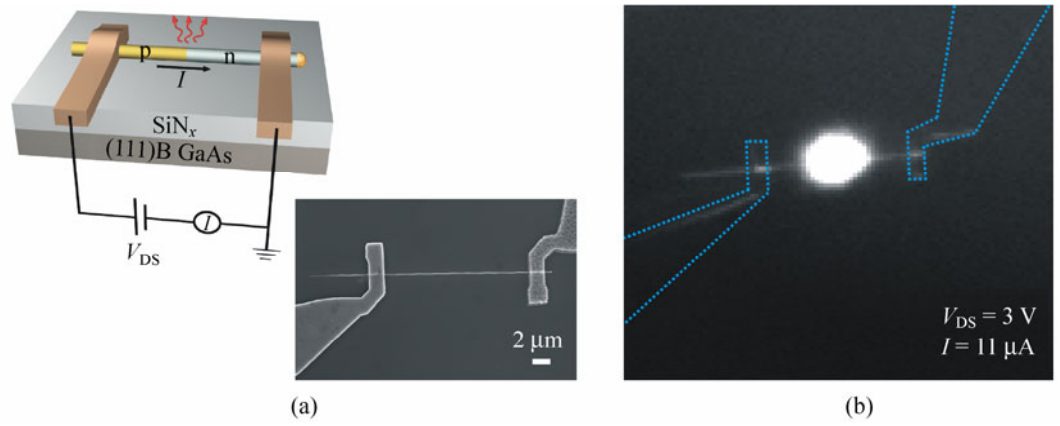

Figure 1 (a) Schematic illustration of the setup for spatially resolved electroluminescence investigations. The lower inset shows a SEM micrograph of the investigated nanowire diode D1. (b) Optical microscope image of the nanowire pn-diode showing pronounced electroluminescence at 300 K under forward bias of 3 V. The electrical contacts to the nanowire device are indicated by dashed lines

and originates from band-to-band recombination at the pn-junction as discussed in detail elsewhere [24]. A pronounced room temperature electroluminescence indicates the high crystalline quality of the axial pn-nanowire diode.

In order to directly visualize the axial doping transition in the pn-nanowire diode and to get access to the local voltage drop in the operating device, Kelvin probe force microscopy (KPFM) [25] was used. This technique allows access to the contact potential difference (CPD) between a tip and the device without any mechanical contact. As the CPD depends on both the work function difference between the tip and the sample, as well as the applied voltage bias to the sample, the potential distribution along the nanowire and thus the local voltage drop can be extracted [26, 27]. In fact, KPFM has been used to measure potential profiles of biased pn-junctions [26, 27], to localize and analyze doping transitions in Ⅲ–Ⅴ nanowires [28, 29] and to determine quantitatively the doping distribution along the axial and radial direction of VLS-grown silicon nanowires [30, 31].

The measurements were performed on a nanowire device D2 under an applied bias as schematically shown in Fig. 2(a). The voltage was applied to the p-contact, while the n-contact was grounded. The topography (Fig. 2(b)) shows the nanowire between the n- and the p-contact on the left and the right side, respectively. The nanowire showed no tapering, meaning that the nanowire diameter for this device (~100 nm) was constant over the whole nanowire length (~12.5 μm). Additionally, no topographic features can be seen between the contacts, meaning that changes observed in the KPFM measurement are caused only by changes in the electronic properties of the nanowire. Figure 2(c) (top) shows the simultaneously measured Kelvin voltage for the same area as shown in the topography plot (Fig. 2(b)). The nanowire was measured under reverse bias, i.e., –2 V was applied to the p-contact. A sharp contrast in the Kelvin voltage distribution between the n-doped and the p-doped parts of the nanowire can be seen, enabling us to localize the position of the pn-junction with an accuracy of less than 50 nm. This can be seen more clearly in the lower part of Fig. 2(c), where an enlarged line scan of the Kelvin voltage distribution is depicted for the area around the pn-junction. From the derivative of the Kelvin voltage we are able to extract the local electric field and thus the extension of the depletion region under reverse bias can be estimated (see inset of Fig. 2(c)) [32]. A value of approximately 540 nm is obtained.

We then operated the device D2 at different bias voltages ranging from –2 V to +2 V and recorded the potential distribution along the nanowire by KPFM. The local voltage drop can be achieved by subtracting the Kelvin voltage distribution for the unbiased case (i.e., when all contacts are grounded) from the Kelvin voltage profiles obtained with an applied bias [26, 27, 33]. The result is shown in Fig. 3, where the voltage

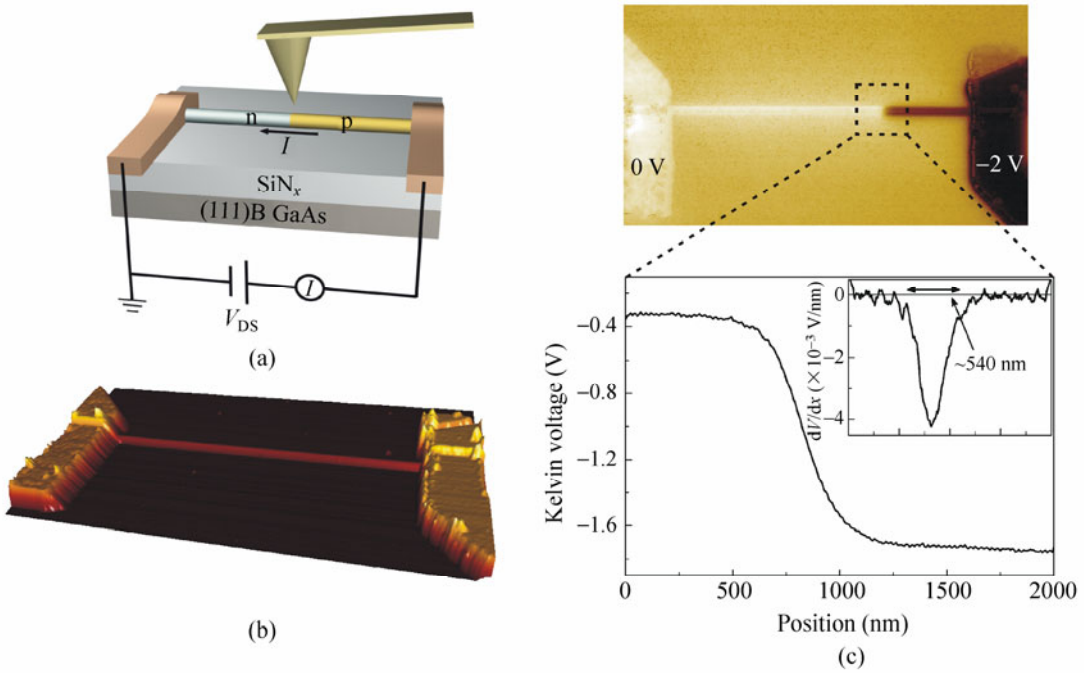

Figure 2 (a) Schematic setup for the KPFM measurements. The n-contact was grounded, while the bias was applied to the p-contact of the nanowire. (b) Topography of the contacted single nanowire diode D2. (c) Kelvin voltage, measured simultaneously with the topography. The n-contact is on the left side and the p-contact on the right side. The measured area shown is 9 μm × 16.5 μm. The color scale for topography and Kelvin voltage represents 520 nm and 2.9 V, respectively. The lower part of (c) shows a line scan of the KPFM measurements obtained in the vicinity of the pn-junction for reverse bias (–2 V). The inset represents the derivative of the Kelvin voltage and shows a depletion length of about 540 nm

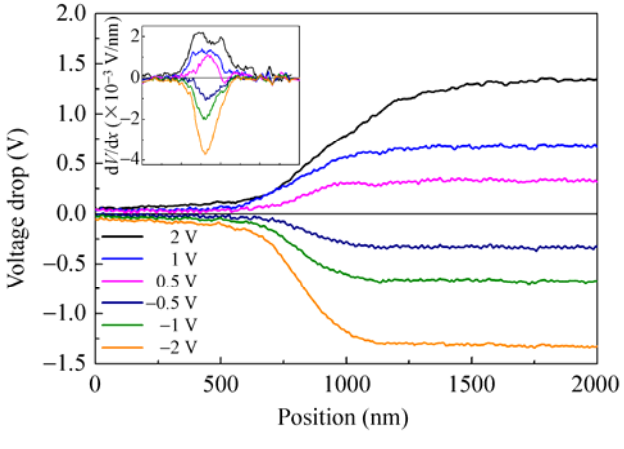

Figure 3 Plots of local voltage drop versus tip position for various applied biases (device D2) in reverse and forward directions. The voltage drop was calculated by subtracting the Kelvin voltage obtained at zero bias from the measured Kelvin voltage profiles obtained under applied bias. The inset shows the derivative of the voltage profiles and reveals that the voltage drop is more localized for reverse bias than in case of forward bias

drop along the nanowire is depicted for the same region as in Fig. 2(c).

It is obvious that for all biases, in reverse as well as in forward directions, the voltage mainly drops in the region of the pn-junction. Again, the derivatives of the measured voltage drop were calculated and plotted against the nanowire position in order to get access to the local electric field extension (see inset of Fig. 3). As expected, the lateral extension of the field along the wire, which is controlled by the space charge region, increases with increasing reverse bias. A significant enhancement of the field extension is obtained in the forward direction, in contradiction to what is expected for an ideal abrupt pn-junction. We attribute this to a deviation from an abrupt junction, e.g., caused by the presence of a small compensated region, resulting in an additional serial resistance becoming important if the device is operated under forward bias. The presence of the compensated region in the axial GaAs nanowire diodes is believed to originate from the memory effect of the Au-seed during VLS growth. This is in agreement with previous investigations using spatially resolved photoluminescence [24].

After proving the high quality of the axial pn-junction in the GaAs nanowires, we are now in a position to evaluate the photoelectric response of the devices and to estimate their potential for PV applications. For this purpose, we performed spatially resolved photocurrent spectroscopy in order to gain access to the mechanism of carrier photogeneration in the nanowire pn-diodes. The ideality factor n of the investigated device was estimated from $I = I_0 \exp(q \cdot V_{\text{bias}} / nkT)$ to be 1.9 in the low voltage range. The $I(V)$ characteristics of the nanowire pn-diode D1 were measured, while the nanowire was locally illuminated by a focused continuous wave (CW) laser (λ = 532 nm) at different positions (Fig. 4(a)). The laser light was focused by an objective lens with a numerical aperture (NA) of 0.5 yielding a spot diameter of ~1.5 μm. The step size was reduced at the expected position of the pn-junction, to achieve higher measurement resolution.

As can be seen in Fig. 4(b), the photocurrent is maximal when the nanowire is illuminated directly at the position of the pn-junction (position 5 in Fig. 4(a)). This correlates nicely with the position of maximum electroluminescence (Fig. 1(b)), observed at the same device. No photocurrent was detected either in the vicinity of the contacts or in the p- and n-doped areas of the diode for any device investigated in this study. This demonstrates that charge separation by an electric field takes place only in the vicinity of the depletion region, while the p- and n- doped nanowire regions are field-free and the contacts have pronounced ohmic character. The estimated length corresponding to the distance between positions 4 and 6 in active absorption device was 1.8 μm. The absorption device length is composed of a depletion region extension as visualized by KPFM, and diffusion lengths of minority carriers, which lie in the range of 0.7–1 μm for highly doped GaAs [34, 35]. The area of 1.8 μm × 200 nm is considered as the active absorption area in the subsequent calculations.

The charge separation efficiency was estimated from $\eta = I/(q \cdot \phi)$, where ϕ is the absorbed photon flux, I is the photocurrent and q is the elementary charge. The number of photons absorbed by the nanowire per second was estimated to be 1.6×10^{12} s^{-1}. The photon flux ϕ absorbed by the nanowire was estimated from the relation $\phi = Q_{\text{abs}} \cdot I_0 \cdot \alpha \cdot \pi \cdot r_{\text{NW}}^2 \cdot d_{\text{laser}} / h\nu$ adopted from Ref. [36] and modified to account for the light scattered by the nanowire. Here $\alpha = 10^5$ cm^{-1} is the absorption coefficient of GaAs at 532 nm [37], r_{NW} = 100 nm is the radius of the investigated nanowire and d_{laser} = 1.5 μm is the diameter of the laser spot and I_0 = 152 W/cm^2 is the incident laser power density. Q_{abs} = 0.8 is the

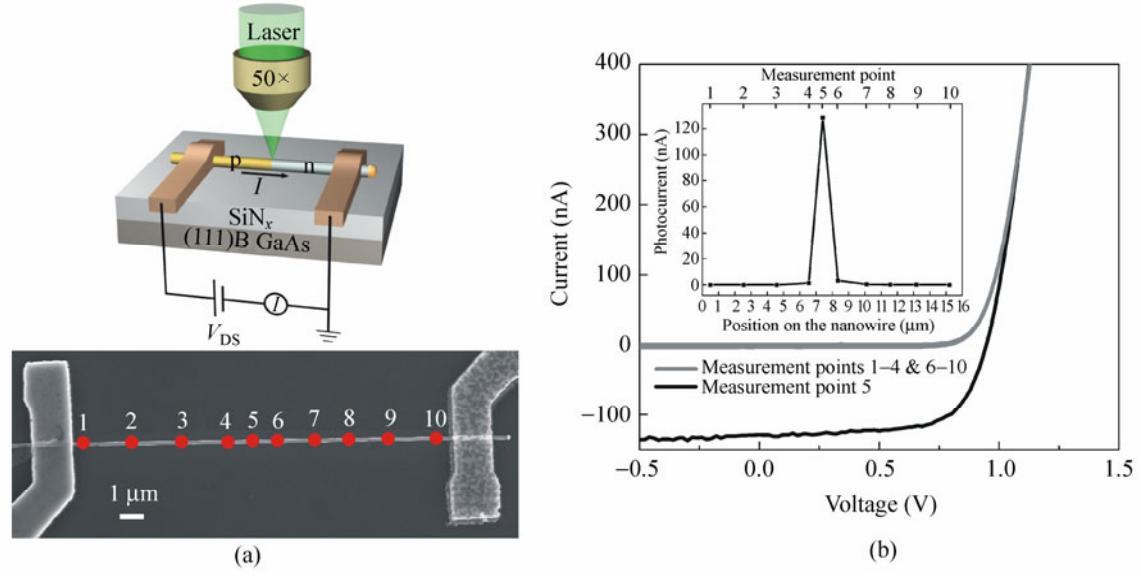

Figure 4 (a) Schematic illustration of the setup for photocurrent microscopy. The lower picture shows a SEM micrograph of the investigated nanowire D1 with the contacts. (b) $I(V)$ characteristics of the GaAs nanowire pn-diode illuminated by a focused laser spot at different positions. $I(V)$ curves from all positions except for position 5 are superimposed. The upper inset shows the photocurrent as a function of the laser spot position. The corresponding positions are denoted by numbers on the SEM image in (a)

absorption efficiency calculated using the Mie theory for an infinite right circular cylinder [38], nonpolarised monochromatic light ($\lambda = 532$ nm) and the case of perpendicular illumination. More details about the calculation of absorption efficiencies for the nanowires can be found in Ref. [39]. The maximum photocurrent at the position of the pn-junction was $I = 128$ nA, yielding a charge separation efficiency of 50%. The charge separation is limited by the recombination of carriers during transport to the contacts via radiative recombination as well as non-radiative losses due to surface traps. The other feature degrading charge separation is the Fermi level pinning at the nanowire surface and the resulting surface depletion region. Note that these factors limiting the effective charge separation in the nanowire PV device can be significantly improved by reducing the wire length and/or by coating the nanowire surface with a passivation shell, as demonstrated in [40].

To determine the solar conversion efficiency of the fabricated nanowire photovoltaic device, $I(V)$ measurements under standard AM 1.5 G conditions provided by a Voss Electronic solar simulator operating with 100 mW/cm^2 (1-sun) illumination intensity were carried out (Fig. 5(a)). A short circuit current of 88 pA and an open circuit voltage of 0.56 V were obtained yielding a fill factor of 69% under 1-sun conditions. Assuming that only the active absorption area contributes to the photocurrent, an apparent short circuit density of 24 mA/cm^2 was obtained. The achieved fill factor of 69% is similar to the value of 65% reported for a single GaAs coaxial nanowire pn-diode [17].

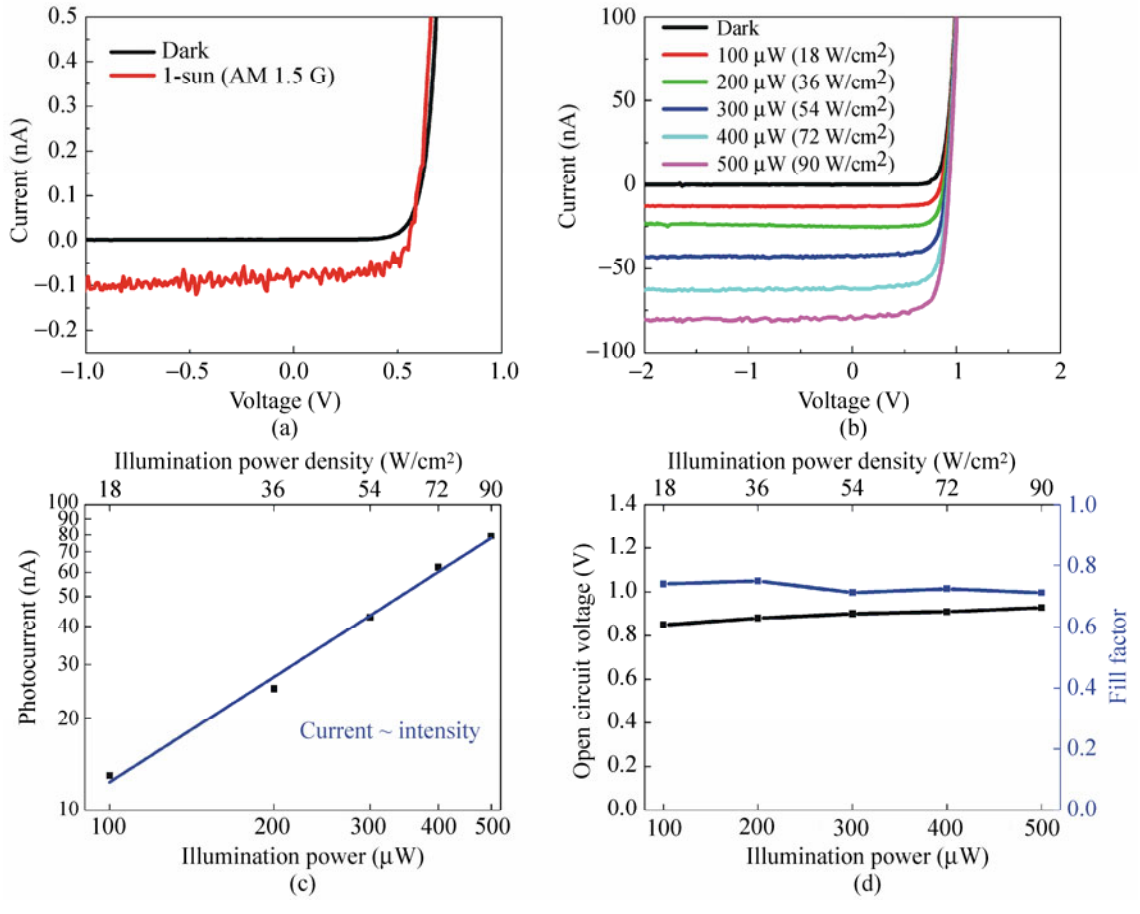

Figure 5 (a) Dark and 1-sun homogeneously illuminated $I(V)$ characteristics of nanowire pn-diode D1. (b) $I(V)$ characteristics of the nanowire pn-diode D1 measured under monochromatic homogeneous laser illumination ($\lambda = 532$ nm) for various illumination power densities. (c) Photocurrent as a function of illumination power ($\lambda = 532$ nm). The line is a linear fit to the data. (d) Power dependence of the open circuit voltage and the fill factor measured under monochromatic homogeneous laser illumination ($\lambda = 532$ nm)

The power conversion efficiency of the nanowire photovoltaic device under standard illumination was estimated using the formula $\eta = V_{oc} \cdot I_{sc} \cdot FF / P_{in}$ to be 9%. P_{in} was calculated from the product of the illumination power density with the active projected absorption area of the nanowire device. This power conversion efficiency is one of the best reported values for a nanowire photovoltaic device. Estimation of the photovoltaic efficiency of a single nanowire device based on the active projected absorption area as obtained by scanning photocurrent microscopy is commonly used by many research groups [9–12, 17]. If, instead, an overall projected area of the device (16 μm × 200 nm) was used for the estimation, the conversion efficiency would be 1%. This value represents the lower bound for our devices.

To investigate the photovoltaic properties of the nanowire diodes under homogeneous higher illumination intensities, the laser spot was expanded to 26.6 μm so that it covered the whole nanowire device with a homogenous laser illumination (λ = 532 nm). Power-dependent photocurrent measurements (Fig. 5(b)) demonstrated the linear scaling of photocurrent with illumination intensity (Fig. 5(c)). This demonstrates that the photosensitivity of the nanowire diode does not change with increasing photoexcitation. The photocurrent follows the increasing photoexcitation with 0.24 A/W up to an illumination density of at least 90 W/cm^2. The remarkably large open circuit voltage of 0.85 V remains almost constant over the entire intensity range (Fig. 5(d)), representing the maximal achievable photovoltage. This value is larger than that (V_{oc} = 0.56 V) measured under 1-sun conditions, demonstrating that saturation of the open circuit voltage was reached within the investigated intensity range.

The fill factor is virtually independent of the illumination power and stays at the level of ~72% (Fig. 5(d)). The independence of the open circuit voltage and fill factor with respect to the illumination power in the investigated high intensity range is technically important for application in concentrator solar cells. It should be noted that the maximum photovoltage is lower than the bandgap of GaAs at room temperature (1.4 eV). The open circuit voltage is a measure of recombination in the nanowire pn-junction and has been shown to be strongly dependent on the surface trap density for single nanowire diodes [41]. For that reason, reduction of both the surface defect states and the surface depletion effects is the key to increasing the open circuit voltage in future nanowire photovoltaic device.

4. Conclusions

We have investigated the photoelectric performance of axial GaAs nanowire photovoltaic devices grown via VLS growth mode in MOVPE. Nanowire pn-diodes have demonstrated strong electroluminescence directly at the position of the pn-junction. The axial modulation of the doping was visualized by the KPFM technique and a depletion length of about 540 nm could be determined for a reverse bias of –2 V.

Spatially resolved photocurrent microscopy shows that optical generation of carriers took place only in the vicinity of the pn-junction dominating the entire photoresponse of the nanowire photovoltaic device. The charge separation efficiency was estimated to be 42% and power-dependent photocurrent measurements demonstrated a linear scaling of the photocurrent with illumination intensity.

The photovoltaic performance of the fabricated nanowire device was investigated for two operation regimes. Under 1-sun AM 1.5 G illumination conditions, a short circuit current density of about 24 mA/cm^2, an open circuit voltage of 0.56 V, a fill factor of 69% and an energy conversion efficiency of 9% were obtained.

Under homogenous high intensity monochromatic illumination (λ = 532 nm), the photocurrent follows the increasing photoexcitation with 0.24 A/W up to an illumination density of at least 90 W/cm^2. The open circuit voltage of 0.85 V and fill factor of 72% were shown to be independent of the illumination intensity over a broad intensity range, which is important for potential applications in concentrator solar cells.

Further improvement of the photovoltaic performance of axial nanowire pn-diodes can be achieved by passivation of the nanowire surface and fabrication of the contacted nanowire diode arrays in topographies which concentrate light on the junction region. An increase of the open circuit voltage may be attained by the combination of single nanowire pn-diodes into a multijunction nanowire device [10, 12]. The

fundamental performance studies of the single nanowire diodes presented here should promote further development of nanowire-based photovoltaic and photonic devices.

Acknowledgements

This work was supported by the European project NaSoL within the Ziel2.NRW program and the Sonderforschungbereich SFB 445. We thank G. Brönstrup for assistance with theoretical calculations.

Electronic Supplementary Material: The video demonstrates the image sequence of a contacted nanowire pn-diode D1 operating at different forward bias voltages at 300 K. The images were taken with an optical microscope. A liquid N_2-cooled charge-coupled device operating in an imaging mode was used as a detector. To highlight the position of the contacted nanowire the sample was illuminated by scattered light from the side. The video is available in the online version of this article at http://dx.doi.org/10.1007/s12274-011-0155-4.

References

[1] Gudiksen, M. S.; Lauhon, L. J.; Wang, J.; Smith, D. C.; Lieber, C. M. Growth of nanowire superlattice structures for nanoscale photonics and electronics. *Nature* **2002**, *415*, 617–620.

[2] Borg, B. M.; Dick, K. A.; Ganjipour, B.; Pistol, M. -E.; Wernersson, L. -E.; Thelander, C. InAs/GaSb heterostructure nanowires for tunnel field-effect transistors. *Nano Lett.* **2010**, *10*, 4080–4085.

[3] Wallentin, J.; Persson, J. M.; Wagner, J. B.; Samuelson, L.; Deppert, K.; Borgström, M. T. High-performance single nanowire tunnel diodes. *Nano Lett.* **2010**, *10*, 974–979.

[4] Fuhrer, A.; Fröberg, L. E.; Pedersen, J. N.; Larsson, M. W.; Wacker, A.; Pistol, M. -E.; Samuelson, L. Few electron double quantum dots in InAs/InP nanowire heterostructures. *Nano Lett.* **2007**, *7*, 243–246.

[5] Tomioka, K.; Motohisa, J.; Hara, S.; Hiruma, S.; Fukui, T. GaAs/AlGaAs core multishell nanowire-based light-emitting diodes on Si. *Nano Lett.* **2010**, *10*, 1639–1644.

[6] Svensson, C. P. T.; Martensson, T.; Trägardh, J.; Larsson, C.; Rask, M.; Hessman, D.; Samuelson, L.; Ohlsson, J. Monolithic GaAs/InGaP nanowire light emitting diodes on silicon. *Nanotechnology,* **2008**, *19*, 305201.

[7] Garnett, E.; Yang, P. Light trapping in silicon nanowire solar cells. *Nano Lett.* **2010**, *10*, 1082–1087.

[8] Diedenhofen, S. L.; Vecchi, G.; Algra, R. E.; Hartsuiker, A.; Muskens, O. L.; Immink, G.; Bakkers, E. P. A. M.; Vos, W. L.; Rivas, J. G. Broad-band and omnidirectional antireflection coatings based on semiconductor nanorods. *Adv. Mat.* **2009**, *21*, 973–978.

[9] Borgström, M. T.; Wallentin, J.; Heurlin, M.; Fält, S.; Wickert, P.; Leene, J.; Magnusson, M. H.; Deppert, K.; Samuelson, L. Nanowires with promise for photovoltaics. *IEEE J. Sel. Top. Quant. Electron.* **2010**, *99*, 1–12.

[10] Heurlin, M.; Wickert, P.; Fält, S.; Borgström, M. T.; Deppert, K.; Samuelson, L.; Magnusson, M. H. Axial InP nanowire tandem junction grown on a silicon substrate. *Nano Lett.* **2011**, *11*, 2028–2031.

[11] Tian, B.; Zheng, X.; Kempa, T. J.; Fang, Y.; Yu, N.; Yu, G. Huang, J.; Lieber, C. M. Coaxial silicon nanowires as solar cells and nanoelectronic power sources. *Nature*, **2007**, *449*, 885–889.

[12] Kempa, T. J.; Tian, B.; Kim, D. R.; Hu, J.; Zheng, X.; Lieber, C. M. Single and tandem axial p–i–n nanowire photovoltaic devices. *Nano Lett.* **2008**, *8*, 3456–3460.

[13] King, R. R.; Law, D. C.; Edmondson, K. M.; Fetzer, C. M.; Kinsey, G. S.; Yoon, H.; Sherif, R. A.; Karam, N. H. 40% efficient metamorphic GaInP/GaInAs/Ge multijunction solar cells. *Appl. Phys. Lett.* **2007**, *90*, 183516.

[14] van Kouwen, M. P.; van Weert, M. H. M.; Reimer, M. E.; Akopian, N.; Perinetti, U.; Algra, R. E.; Bakkers, E. P. A. M.; Kouwenhoven, L. P.; Zwiller, V. Single quantum dot nanowire photodetectors. *Appl. Phys. Lett.* **2010**, *97,* 113108.

[15] Goto, H.; Nosaki, K.; Tomioka, K.; Hara, S.; Hiruma, K.; Motohisa, J.; Fukui, T. Growth of core–shell InP nanowires for photovoltaic application by selective-area metal organic vapor phase epitaxy. *Appl. Phys. Express*, **2009**, *2*, 035004.

[16] Dong, Y.; Tian, B.; Kempa, T. J.; Lieber, C. M. Coaxial group Ⅲ–Nitride nanowire photovoltaics. *Nano Lett.* **2009**, *9*, 2183–2187.

[17] Colombo, C.; Heiß, M.; Grätzel, M.; Fontcuberta i Morral, A. Gallium arsenide p-i-n radial structures for photovoltaic applications. *Appl. Phys. Lett.* **2009**, *94*, 173108.

[18] Czaban, J. A.; Thompson, D. A.; LaPierre, R. R. GaAs core−shell nanowires for photovoltaic applications. *Nano Lett.* **2009**, *9*, 148–154.

[19] Karam, N. H.; Sherif, R. A.; King, R. R. Multijunction concentrator solar cells: An enabler for low-cost photovoltaic systems. In *Concentrator Photovoltaics;* Luque Lopéz,

A. L.; Andreev, V. M., Eds. Springer: Berlin, 2007; p. 200.

[20] Wanlass, M. W.; Ahrenkiel, S. P.; Ahrenkiel, R. K.; Albin, D. S.; Carapella, J. J.; Duda, A.; Geisz, J. F.; Kurtz, S.; Moriarty, T.; Wehrer, R. J.; Wernsman, B. Lattice-mismatched approaches for high-performance, Ⅲ–Ⅴ, photovoltaic energy converters. In *Proc. 31st IEEE Photovoltaic Specialists Conf.*, Lake Buene Vista, Florida, 2005; pp. 530–535.

[21] Gutsche, C.; Regolin, I.; Blekker, K.; Lysov, A.; Prost, W.; Tegude, F. -J. Controllable p-type doping of GaAs nanowires during vapor–liquid–solid growth. *J. Appl. Phys.* **2009**, *105*, 024305,

[22] Gutsche, C.; Lysov, A.; Regolin, I.; Blekker, K.; Prost, W.; Tegude, F. -J. n-type doping of vapor-liquid-solid grown GaAs nanowires. *Nanoscale Res. Lett.* **2011**, *6*, 65–70.

[23] Regolin, I.; Gutsche, C.; Lysov, A.; Blekker, K.; Li, Z. -A.; Spasova, M.; Prost, W.; Tegude, F. -J. Axial pn-junctions formed by MOVPE using DEZn and TESn in vapour-liquid-solid grown GaAs nanowires. *J. Cryst. Growth* **2011**, *315*, 143–147.

[24] Lysov, A.; Offer, M.; Gutsche, C.; Regolin, I.; Topaloglu, S.; Geller, M.; Prost, W.; Tegude, F. -J. Optical properties of heavily doped GaAs nanowires and electroluminescent nanowire structures. *Nanotechnology,* **2011**, *22*, 085702.

[25] Nonnenmacher, M.; O'Boyle, M. P.; Wickramasinghe, H. K. Kelvin probe force microscopy. *Appl. Phys. Lett.* **1991**, *58*, 2921–2923.

[26] Katzer, Kl. -D.; Mertin, W.; Bacher, G.; Jaeger, A.; Streubel, K. Voltage drop in an $(Al_xGa_{1-x})_{0.5}In_{0.5}P$ light-emitting diode probed by Kelvin probe force microscopy. *Appl. Phys. Lett.* **2006**, *89*, 103522.

[27] Lévêque, G.; Girard, P.; Skouri, E.; Yarekha, D. Measurements of electric potential in a laser diode by Kelvin probe force microscopy. *Appl. Surf. Sci.* **2000**, *157*, 251–255.

[28] Minot, E. D.; Kelkensberg, F.; van Kouwen, M.; van Dam, J. A.; Kouwenhoven, L. P.; Zwiller, V.; Borgström, M.; Wunnicke, O.; Verheijen, M. A.; Bakkers, E. P. A. M. Single quantum dot nanowire LEDs. *Nano Lett.* **2007**, *7*, 367–371.

[29] Vinaji, S.; Lochthofen, A.; Mertin, W.; Regolin, I.; Gutsche, C.; Prost, W.; Tegude, F. J.; Bacher, G. Material and doping transitions in single GaAs-based nanowires probed by Kelvin probe force microscopy. *Nanotechnology* **2009**, *20*, 385702.

[30] Koren, E.; Rosenwaks, Y.; Allen, J. E.; Hemesath, E. R.; Lauhon, L. J. Nonuniform doping distribution along silicon nanowires measured by Kelvin probe force microscopy and scanning photocurrent microscopy. *Appl. Phys. Lett*. **2009**, *95*, 092105.

[31] Koren, E.; Hyun, J. K.; Givan, U.; Hemesath, E. R.; Lauhon, L. J.; Rosenwaks, Y. Obtaining uniform dopant distributions in VLS-grown Si nanowires. *Nano Lett.* **2011**, *11*, 183–187.

[32] Robin, F.; Jacobs, H.; Homan, O.; Stemmer, A.; Bächtold, W. Investigation of the cleaved surface of a p–i–n laser using Kelvin probe force microscopy and two-dimensional physical simulations. *Appl. Phys. Lett.* **2000**, *76*, 2907–2909.

[33] Bürgi, L.; Sirringhaus, H.; Friend, R. H. Noncontact potentiometry of polymer field-effect transistors. *Appl. Phys. Lett.* **2002**, *80*, 2913–2915.

[34] Tiwari, S.; Wright, S. L. Material properties of p-type GaAs at large dopings. *Appl. Phys. Lett.* **1990**, *56*, 563–565.

[35] Liang, B. W.; Zou, Y. X.; Zhou, B. L.; Milnes, A. G. Minority carrier diffusion lengths in bulk n-type GaAs. *J. Elect. Mater.* **1987**, *16*, 177–180.

[36] Graham, R.; Miller, C.; Oh, E.; Yu, D. Electric field dependent photocurrent decay length in single lead sulfide nanowire field effect transistors. *Nano. Lett.* **2011**, *11*, 717–722.

[37] Luque, A.; Hegedus, S. *Handbook of Photovoltaic Science and Engineering;* John Wiley & Sons, 2003; p.73.

[38] Bohren, C.; Huffman, D. R. *Absorption and Scattering of Light by Small Particles;* Wiley-VCH: New York, 1983; pp. 202–213.

[39] Brönstrup, G.; Jahr, N.; Leiterer, C.; Csáki, A.; Fritzsche, W.; Christiansen, S. Optical properties of individual silicon nanowires for photonic devices. *ACS Nano* **2010**, *4*, 7113–7122.

[40] Parkinson, P.; Joyce, H. J.; Gao, Q.; Tan, H. H.; Zhang, X.; Zou, J.; Jagadish, C.; Herz, L. M.; Johnston, M. B. Carrier lifetime and mobility enhancement in nearly defect-free core–shell nanowires measured using time-resolved terahertz spectroscopy. *Nano Lett.* **2009**, *9*, 3349–3353.

[41] LaPierre, R. R. Numerical model of current-voltage characteristics and efficiency of GaAs nanowire solar cells. *J. Appl. Phys.* **2011**, *109*, 034311.